

Color-picture part

4.1.1.4 Solar photosphere and chromosphere

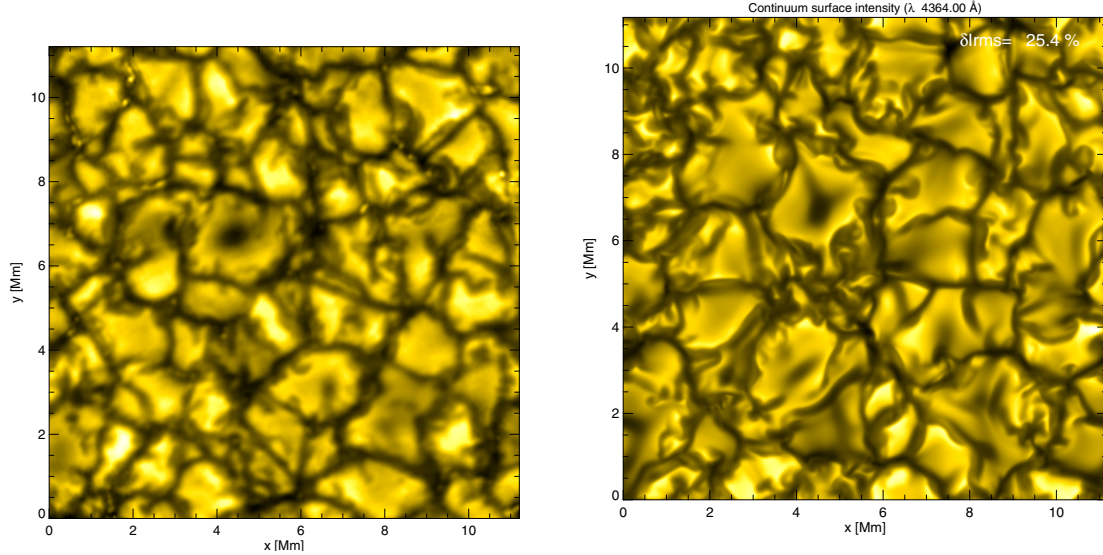


Fig. 12. **Left:** Quiet solar granulation as observed with the 1m Swedish Solar Telescope (courtesy Mats Carlsson 2004). **Right:** High-resolution CO5BOLD simulation of solar surface convection on a $n_x \times n_y \times n_z = 400 \times 400 \times 165$ grid. Both images show the emergent continuum intensity (using identical scaling) at $\lambda 436.4$ nm in a field measuring $15'' \times 15''$ (11×11 Mm). Reproduced from [07Ste1].

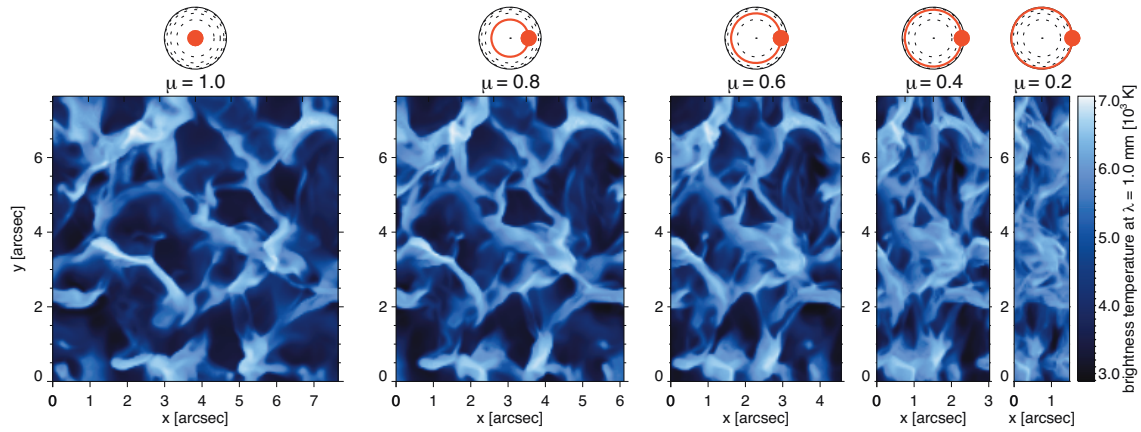


Fig. 19. **Top:** Gas temperature at a geometric height of $z = 1000$ km above $\tau_{\text{Ross}} = 1$ in the nonmagnetic 3D chromospheric model by [04Wed]. Temperatures range from 2000 K (black) to 7000 K (white). **Bottom:** Brightness temperature T_b of synthetic continuum images at $\lambda 1$ mm, computed from the snapshot shown at left for different inclination angles ($\mu = 1$: disk-center, $\mu = 0.2$: close to limb). T_b ranges from 3000 K (black) to 7000 K (white). Adapted from [07Wed3].

4.1.2 Solar activity

4.1.2.1 Active regions

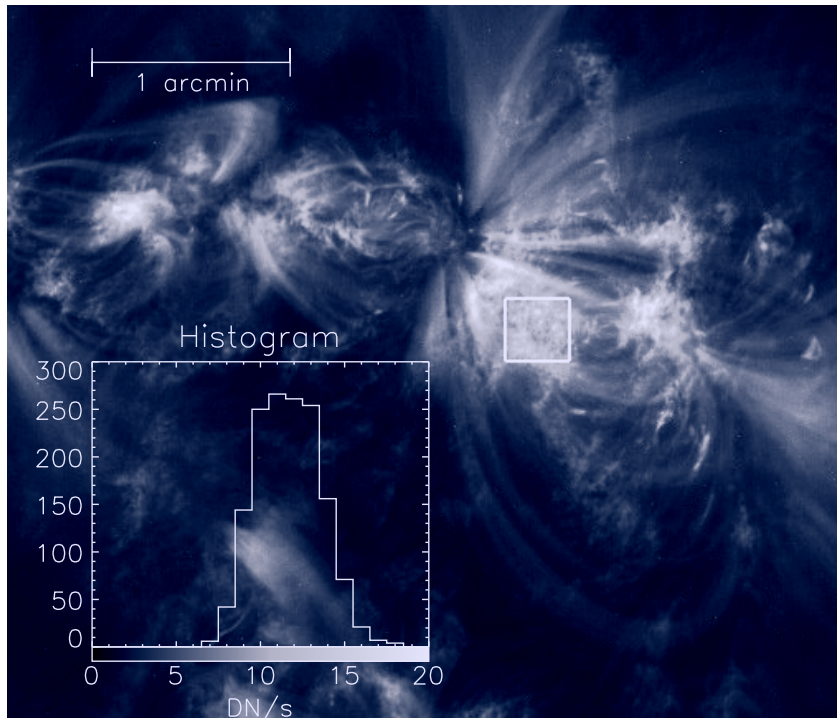


Fig. 2. Moss region observed in the 17.1 nm wavelength band on 6 June 1999. The square box with an angular size of $19'' \times 19''$ contains bright moss structures with a brightness distribution given in the histogram inset. AR loops can be seen in the neighbourhood (from [00Mar]).

4.1.2.2 Solar activity cycle

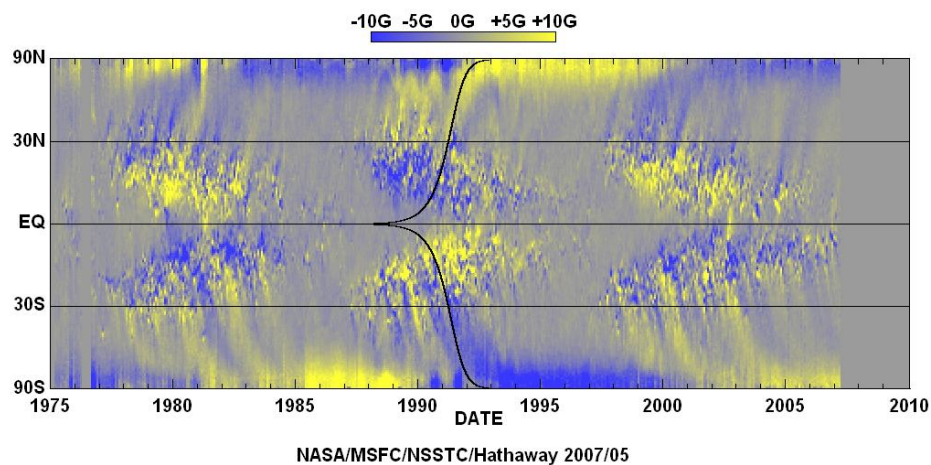


Fig. 5. Butterfly diagram of the radial component of the solar magnetic field [03Hat]. For each Carrington rotation, the magnetic flux is summed in longitude in each latitude bin.

4.1.2.3 Sun spots

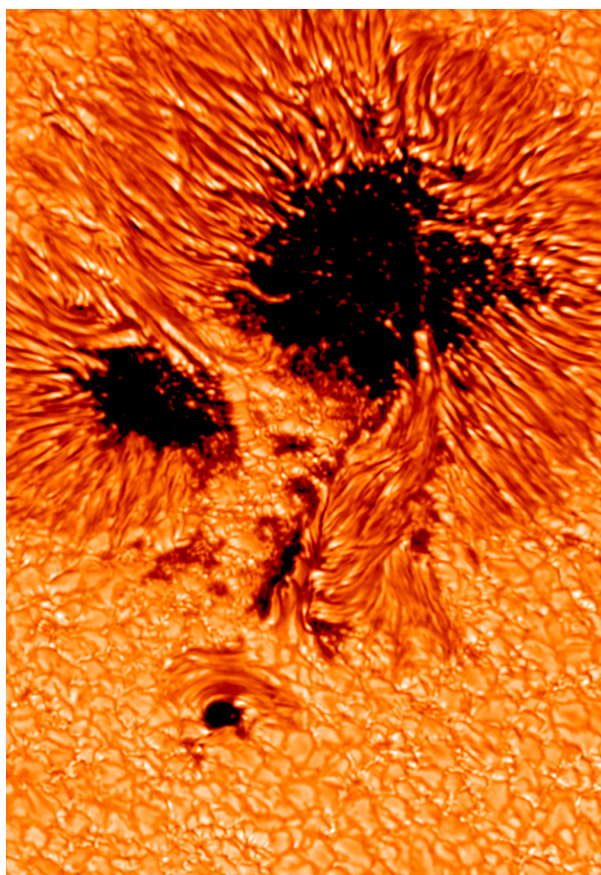


Fig. 1. Image of a complex sunspot with two umbrae observed in the red continuum with the Swedish Solar Telescope on La Palma. With kind permission of J. Hirzberger.

4.1.2.5 Prominences and ejecta

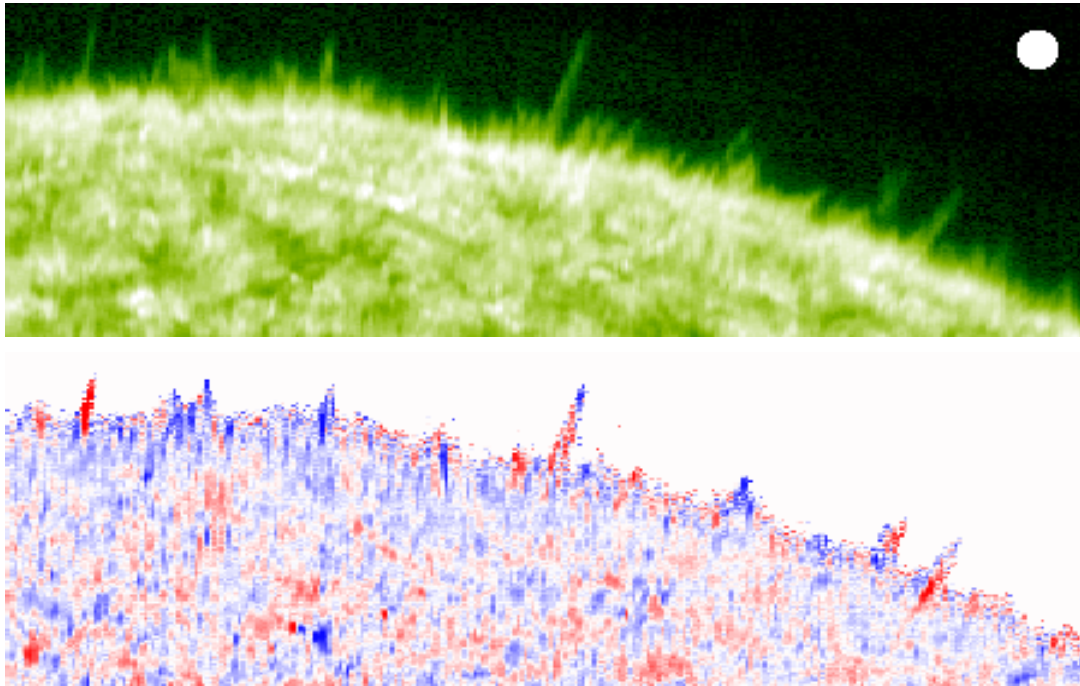


Fig 2. Spicule activity at the solar limb in O V emission at 62.973 nm with the corresponding Doppler diagram in the lower panel. The frame dimensions are 310 Mm \times 100 Mm. The tallest feature protrudes approximately 40 Mm from the limb and is a macrospicule judged by its length. The size of the Earth is shown for comparison in the upper panel.

4.2 The planets and their satellites

4.2.1 Introduction

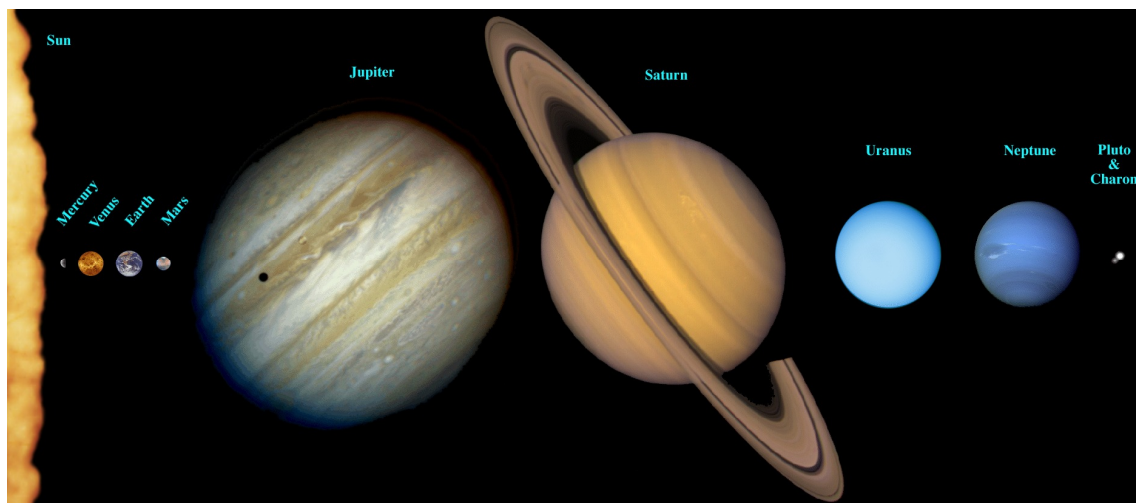


Fig. 1. The eight planets Mercury, Venus, Earth, Mars, Jupiter, Saturn, Uranus, and Neptune are shown with their correct relative sizes (the distances are not to scale). The compilation also includes the dwarf planet Pluto and its moon Charon. The dark spot on Jupiter is the shadow of Io, one of the four Galilean Moons. ©C.J. Hamilton

4.2.3 Terrestrial planets and satellites

4.2.3.1 Geodetic and geophysical data

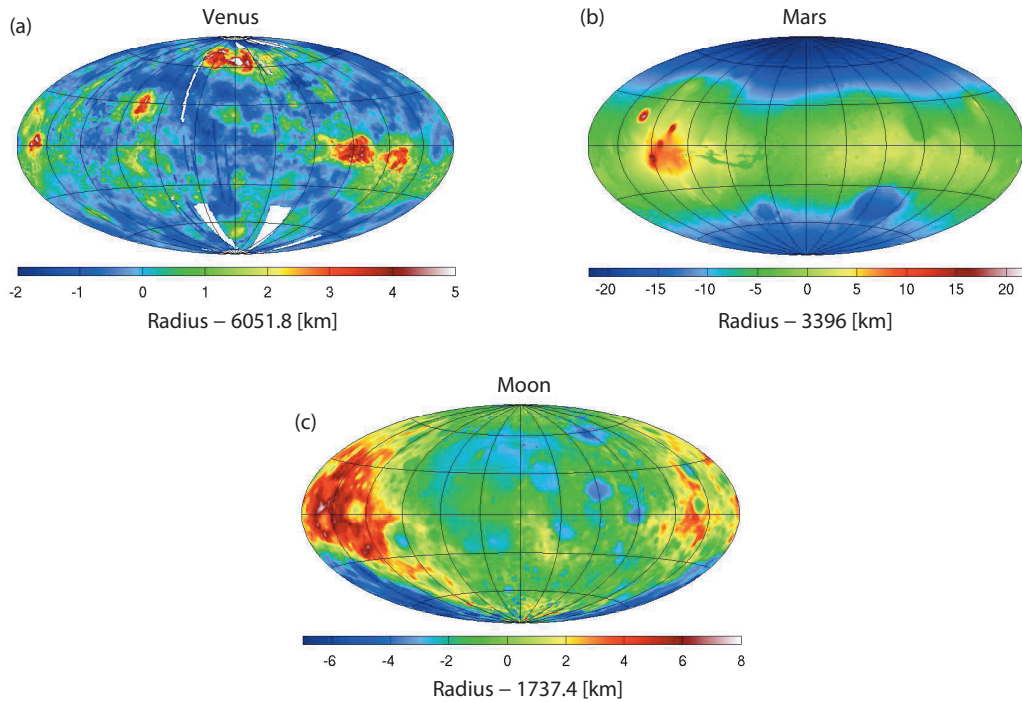


Fig. 2. Planetary radii models of Venus, Mars and the Moon. All images are in a Hammer projection with a central meridian of 0° W. The values are referenced to a sphere of radius 6051.8, 3396 and 1737.4 km for Venus, Mars and the Moon, respectively. Note the data gaps for Venus and the rotational flattening present for Mars.

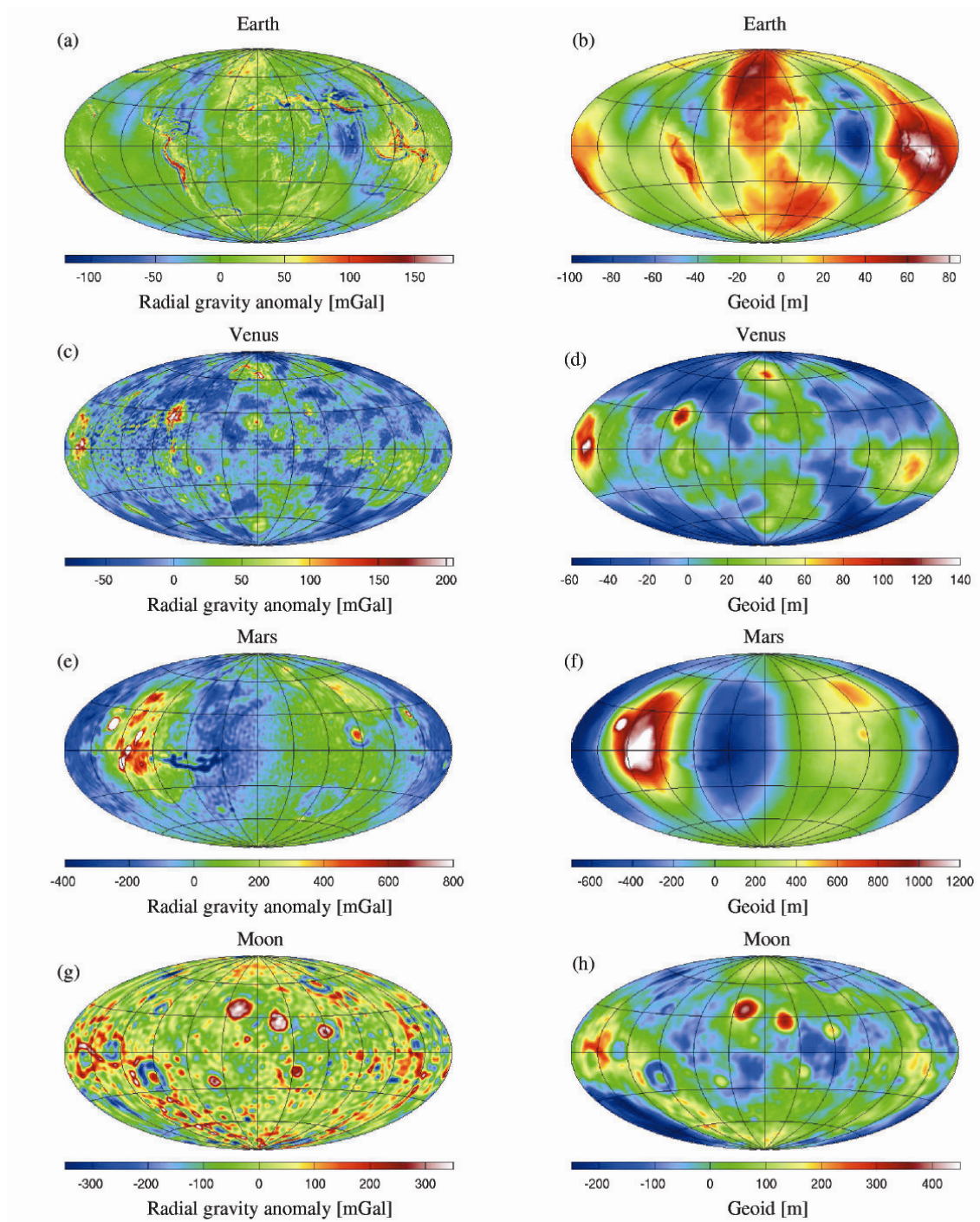


Fig. 3. Radial gravity anomaly g_r and geoid height N for the Earth, Venus, Mars and the Moon. All images are in a Hammer projection with a central meridian of 0° W. (a)-(b) g_r and N for the Earth, evaluating the model EIGEN-GL04C [08För] at a reference radius $R_p = 6378.13$ km and setting the zonal degree-2 term C_{20} to zero. (c)-(d) g_r and N for Venus, evaluating the model SHGJ180 [06Rap] at $R_p = 6051$ km (e)-(f) g_r and N for Mars, evaluating the model MGS95J [05Tyl] at $R_p = 3396$ km and setting the zonal degree-2 term C_{20} to zero. (g)-(h) g_r and N for the Moon, evaluating the model LP165P [97Lem] at $R_p = 1738$ km and setting the zonal degree-2 term C_{20} and C_{22} to zero.